

Supplemental Methods

Electrophysiology - Current recordings were measured by conventional whole-cell patch-clamp technique with an Axon 200B patch-clamp amplifier controlled by a personal computer using a Digidata 1320A acquisition board driven by pClamp 8.0 software (Axon Instruments, Foster City, CA). Electrophysiological recordings were obtained from Ca^{2+} -tolerant, rod-shaped ventricular cells. Whole cell sodium currents were measured in cardiomyocytes using standard protocols as described in detail (1, 2). Briefly, a whole-cell bath solution containing 10 mM NaCl, 130 mM choline chloride, 4.5 mM KCl, 1.8 mM CaCl_2 , 2.0 mM MgCl_2 , 10.0 mM Hepes, and 5.5 mM glucose, pH 7.35, titrated with KOH. The pipette solution contained 130 mM CsCl, 0.5 mM CaCl_2 , 2 mM MgCl_2 , 5 mM Na_2ATP , 0.5 mM GTP, 5 mM EGTA, and 10 mM Hepes, pH 7.3, titrated with CsOH. Current recordings were low-pass filtered at 5 kHz and digitized at a sampling rate of 20 kHz. Standard protocols were used to measure current-voltage relationship, steady-state inactivation, recovery from inactivation (1) and late current as described by Wagner, Bers, and Maier (2). To ensure that whole cell measurements represented total I_{Na} in the myocyte, measurements were generally performed on smaller capacitance cells (~80-90 pF) to ensure adequate space clamp conditions. However, we observed equal I_{Na} density in smaller and larger (~120 pF) capacitance cells (Supplemental Figure 11) confirming our ability to measure total available I_{Na} in our experiments. As previously described by George and colleagues, cells exhibiting very large whole-cell currents were excluded if voltage-control was compromised (3). Calcium currents were measured using an intracellular solution containing (in mM): CsCl 120, CaCl_2 3, tetraethylammonium chloride 10, MgATP 1, NaGTP 1, phosphocreatine 5, HEPES 10, and EGTA 10, titrated to pH 7.2 with 1 M CsOH. The cells were bathed in 137 mM NMDG, 10 mM HEPES, 10 mM glucose, 1.8 mM CaCl_2 , 0.5 mM MgCl_2 , and 25 mM CsCl titrated to pH 7.4 with 12.1 M HCl. Ca^{2+} current facilitation was measured as described previously(4). All current recording experiments were conducted at room temperature (21-23 °C). Recording pipettes, fabricated from borosilicate glass, had resistance of 2-4 M Ω , when filled with recording solution. All solutions were adjusted to 275-295 mOsm. Ito and total myocyte K current was measured as described by Nerbonne and colleagues (5).

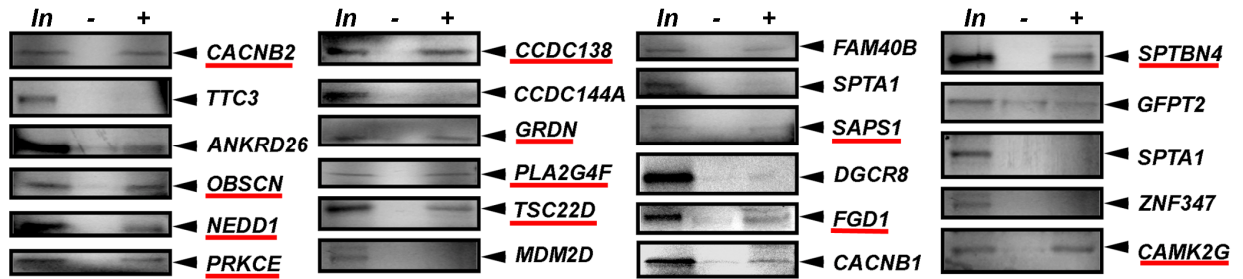
Electrocardiograms – ECGs were recorded *in vivo* or *ex vivo* from Langendorff-perfused hearts as described in detail by Mitchell, Jeron, and Koren (6) and Casimiro, Knollmann and Pfeifer (7) but also by our group(8, 9). Briefly, continuous recordings were collected for each mouse but only ECG complexes with clearly defined onset and termination signals were sampled. ECG parameter measurement was performed by one individual and confirmed by a second. Standard criteria were used to measure ECG parameters (RR interval, QRS duration, etc.) (6, 10). Mice have a biphasic T-wave (6, 11) consisting of a rapid initial component (T_r) and a late slower component (T_s). QT intervals have been reported in mice using either T_r (time for return of T to isoelectric line) or end of biphasic T wave ($T_r + T_s$) (6, 11-15). *qv3J* mice had decreased QT interval (QT90) using either criteria).

References for Supplemental Methods

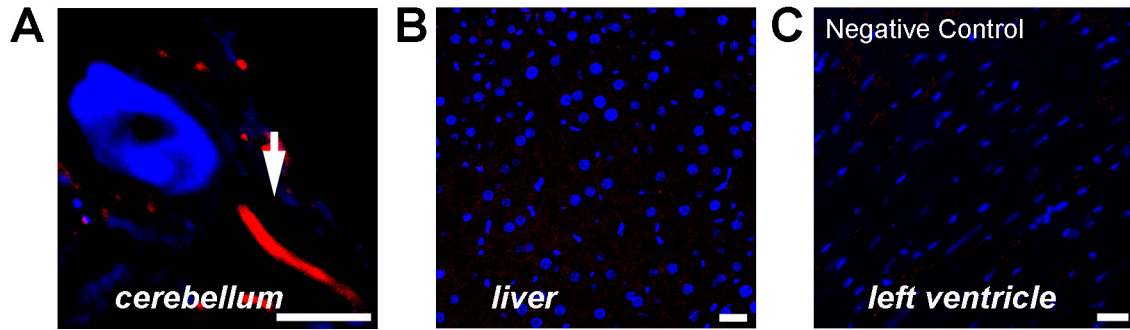
1. Lowe, J.S., Palygin, O., Bhasin, N., Hund, T.J., Boyden, P.A., Shibata, E., Anderson, M.E., and Mohler, P.J. 2008. Voltage-gated Nav channel targeting in the heart requires an ankyrin-G dependent cellular pathway. *J Cell Biol* 180:173-186.
2. Wagner, S., Dybkova, N., Rasenack, E.C., Jacobshagen, C., Fabritz, L., Kirchhof, P., Maier, S.K., Zhang, T., Hasenfuss, G., Brown, J.H., et al. 2006. Ca^{2+} /calmodulin-dependent protein kinase II regulates cardiac Na^+ channels. *J Clin Invest* 116:3127-3138.

3. Wang, D.W., Desai, R.R., Crotti, L., Arnestad, M., Insolia, R., Pedrazzini, M., Ferrandi, C., Vege, A., Rognum, T., Schwartz, P.J., et al. 2007. Cardiac sodium channel dysfunction in sudden infant death syndrome. *Circulation* 115:368-376.
4. Wu, Y., Dzura, I., Colbran, R.J., and Anderson, M.E. 2001. Calmodulin kinase and a calmodulin-binding 'IQ' domain facilitate L-type Ca²⁺ current in rabbit ventricular myocytes by a common mechanism. *J Physiol* 535:679-687.
5. Xu, H., Guo, W., and Nerbonne, J.M. 1999. Four kinetically distinct depolarization-activated K⁺ currents in adult mouse ventricular myocytes. *J Gen Physiol* 113:661-678.
6. Mitchell, G.F., Jeron, A., and Koren, G. 1998. Measurement of heart rate and Q-T interval in the conscious mouse. *Am J Physiol* 274:H747-751.
7. Casimiro, M.C., Knollmann, B.C., Ebert, S.N., Vary, J.C., Jr., Greene, A.E., Franz, M.R., Grinberg, A., Huang, S.P., and Pfeifer, K. 2001. Targeted disruption of the *Kcnq1* gene produces a mouse model of Jervell and Lange-Nielsen Syndrome. *Proc Natl Acad Sci U S A* 98:2526-2531.
8. Li, J., McLerie, M., and Lopatin, A.N. 2004. Transgenic upregulation of IK1 in the mouse heart leads to multiple abnormalities of cardiac excitability. *Am J Physiol Heart Circ Physiol* 287:H2790-2802.
9. Mohler, P.J., Schott, J.J., Gramolini, A.O., Dilly, K.W., Guatimosim, S., duBell, W.H., Song, L.S., Haurogne, K., Kyndt, F., Ali, M.E., et al. 2003. Ankyrin-B mutation causes type 4 long-QT cardiac arrhythmia and sudden cardiac death. *Nature* 421:634-639.
10. Papadatos, G.A., Wallerstein, P.M., Head, C.E., Ratcliff, R., Brady, P.A., Benndorf, K., Saumarez, R.C., Trezise, A.E., Huang, C.L., Vandenberg, J.I., et al. 2002. Slowed conduction and ventricular tachycardia after targeted disruption of the cardiac sodium channel gene *Scn5a*. *Proc Natl Acad Sci U S A* 99:6210-6215.
11. Lande, G., Demolombe, S., Bammert, A., Moorman, A., Charpentier, F., and Escande, D. 2001. Transgenic mice overexpressing human KvLQT1 dominant-negative isoform. Part II: Pharmacological profile. *Cardiovasc Res* 50:328-334.
12. Berul, C.I., Aronovitz, M.J., Wang, P.J., and Mendelsohn, M.E. 1996. In vivo cardiac electrophysiology studies in the mouse. *Circulation* 94:2641-2648.
13. Demolombe, S., Lande, G., Charpentier, F., van Roon, M.A., van den Hoff, M.J., Toumaniantz, G., Baro, I., Guihard, G., Le Berre, N., Corbier, A., et al. 2001. Transgenic mice overexpressing human KvLQT1 dominant-negative isoform. Part I: Phenotypic characterisation. *Cardiovasc Res* 50:314-327.
14. Itokawa, K., Sora, I., Schindler, C.W., Itokawa, M., Takahashi, N., and Uhl, G.R. 1999. Heterozygous VMAT2 knockout mice display prolonged QT intervals: possible contributions to sudden death. *Brain Res Mol Brain Res* 71:354-357.
15. London, B., Jeron, A., Zhou, J., Buckett, P., Han, X., Mitchell, G.F., and Koren, G. 1998. Long QT and ventricular arrhythmias in transgenic mice expressing the N terminus and first transmembrane segment of a voltage-gated potassium channel. *Proc Natl Acad Sci U S A* 95:2926-2931.

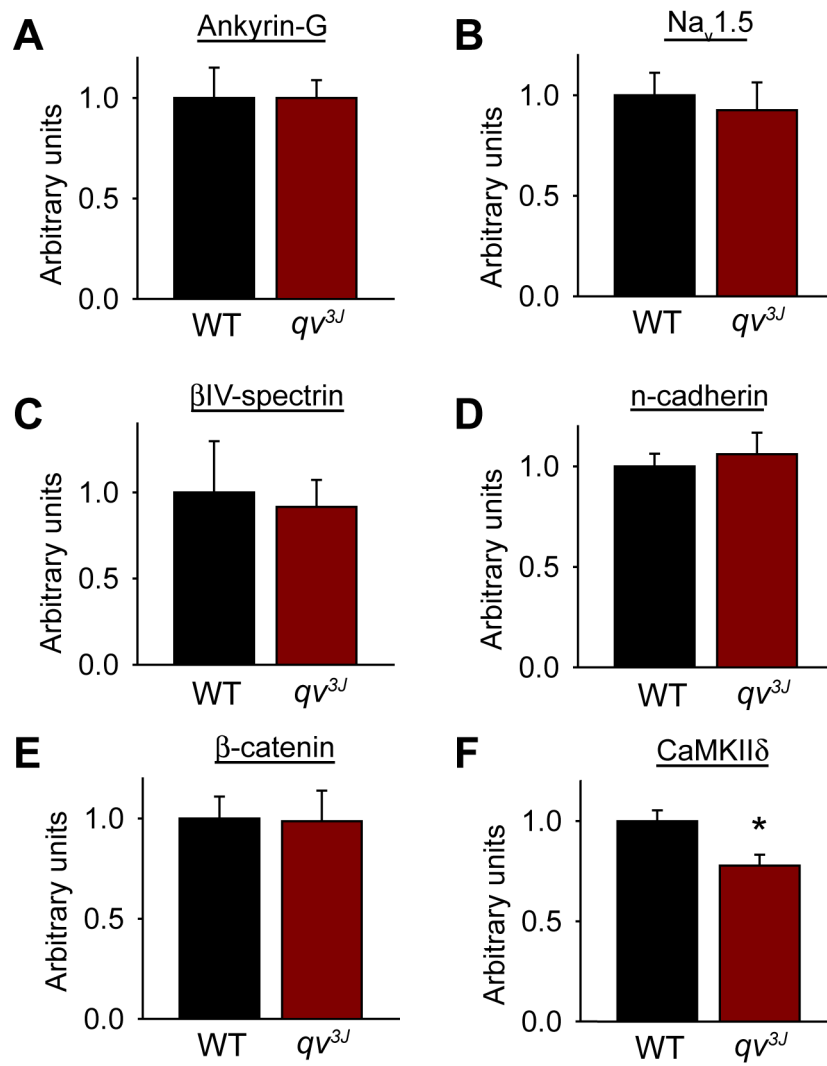
Supplemental Fig. 1



Supplemental Fig. 2

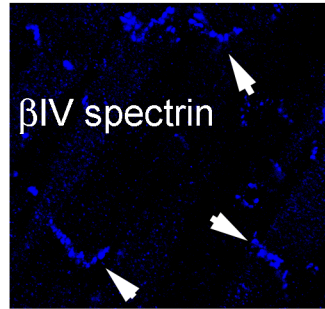


Supplemental Fig. 3

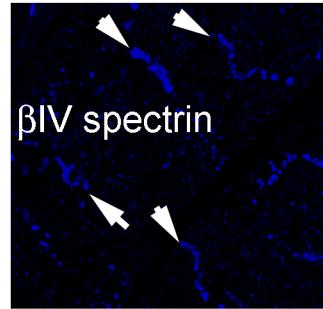


Supplemental Fig. 4

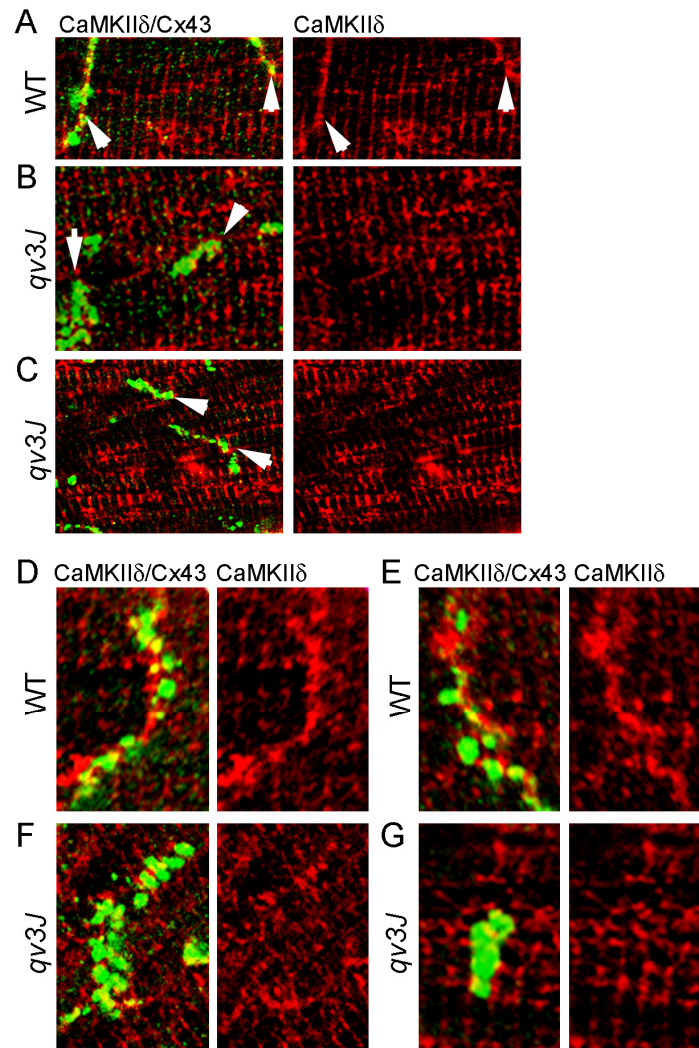
A WT



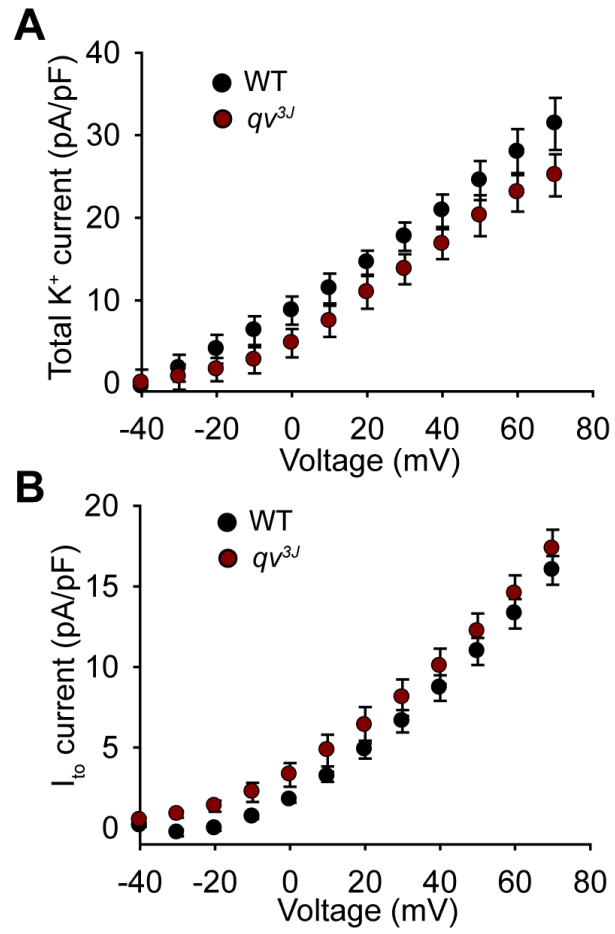
B $qv3J$



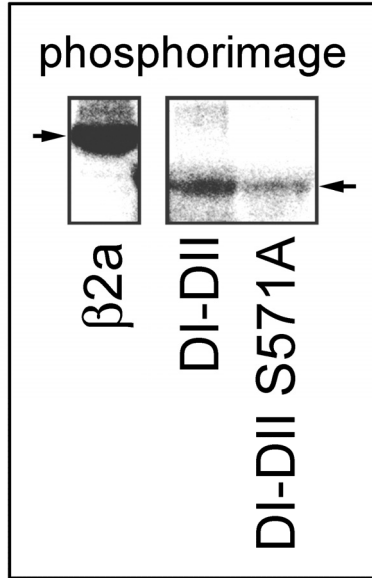
Supplemental Fig. 5



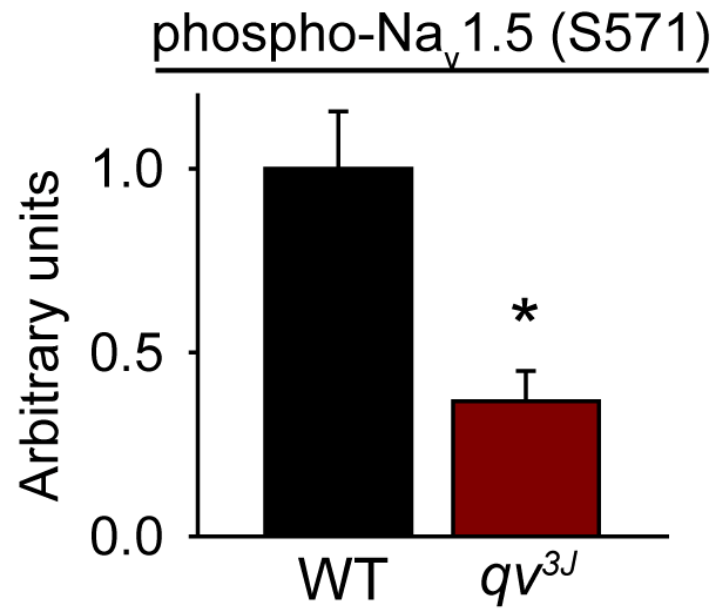
Supplemental Fig. 6



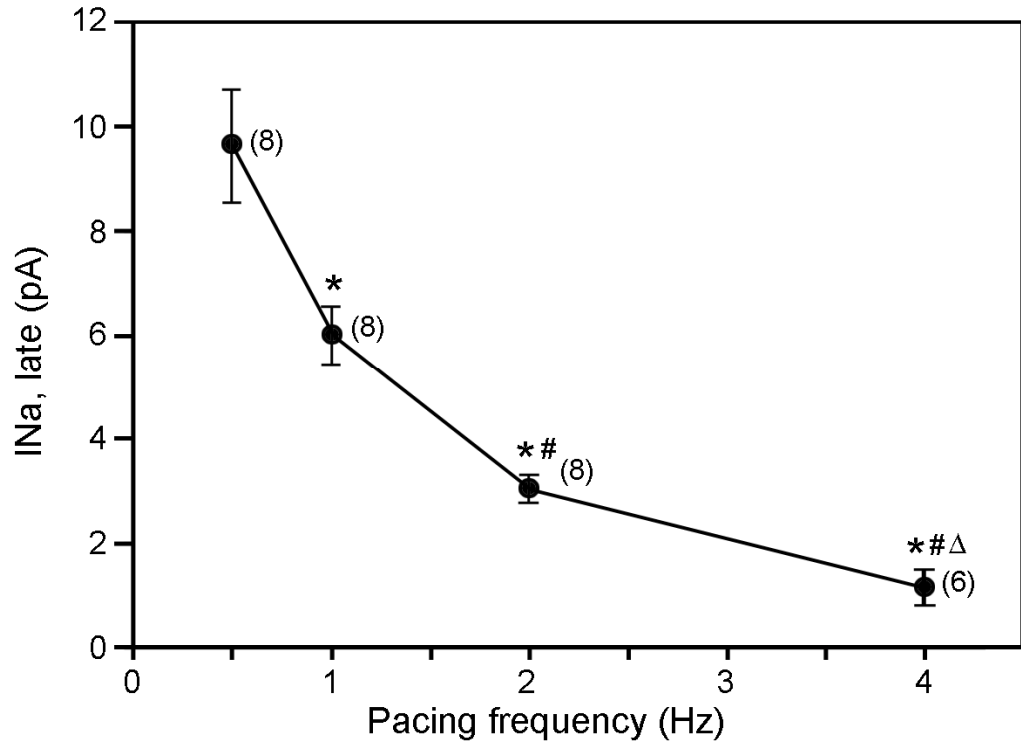
Supplemental Fig. 7



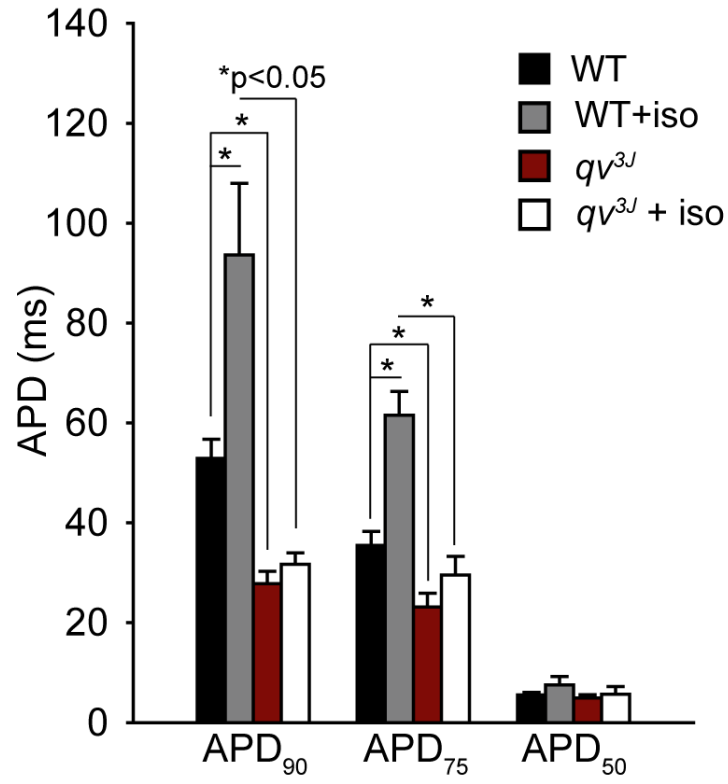
Supplemental Fig. 8



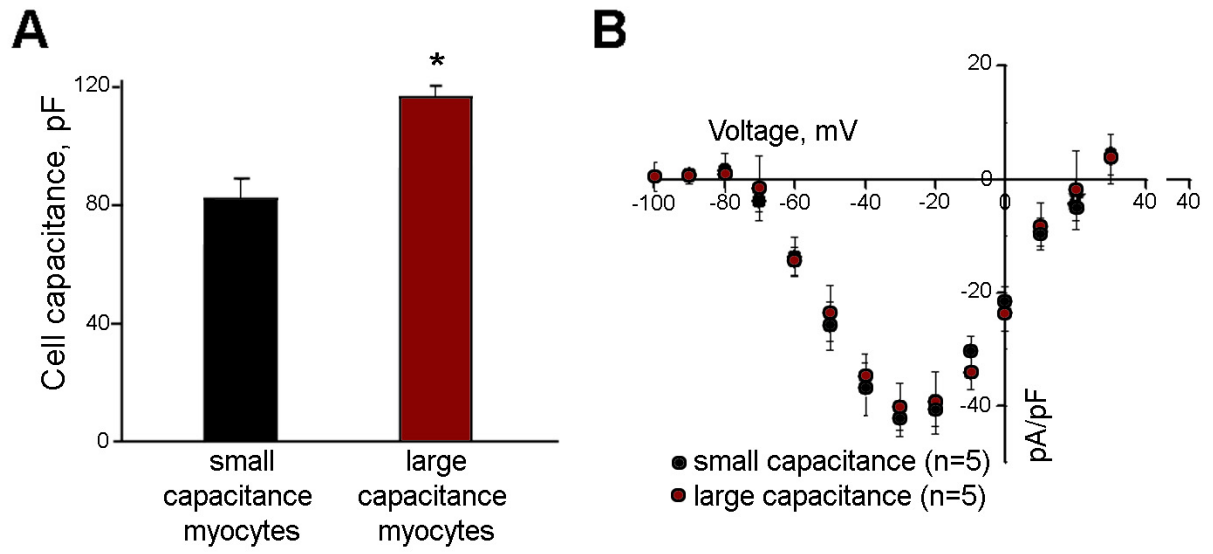
Supplemental Fig. 9



Supplemental Fig. 10



Supplemental Fig. 11



Supplemental Figure Legends

Figure S1. Identification of novel CaMKII binding partners *in vitro*. Candidates were cloned from human tissue and CaMKII-binding activity was assessed by *in vitro* binding assays using radiolabeled target proteins and activated CaMKII (CaMKII T287D). Only twelve clones showed remarkable CaMKII-binding activity in this assay. Blots are labeled with In (Input), - (control Ig), and + (CaMKII Ig). Red lines denote clones that showed robust binding for CaMKII in repeated experiments.

Figure S2. β_{IV} -spectrin immunostaining in mouse tissue. Immunostaining of β_{IV} -spectrin in mouse **(A)** cerebellar Purkinje neurons and **(B)** liver. Note that in **(A)** β_{IV} -spectrin (*red*) is strongly localized to the Purkinje cell axon initial segment (arrowhead, blue staining denotes calbindin), whereas no specific β_{IV} -spectrin immunostaining (*red*) was observed in liver (negative control, nuclei are stained in *blue*). **(C)** Mouse left ventricle immunolabeled with secondary antibody alone (Negative control). Nuclei are immunolabeled with topro-3AM (*blue*). Scale bars equal 10 microns for **A**, and 30 microns for **B-C**.

Figure S3. Expression of select myocyte proteins in WT and qv^{3J} heart. Equal quantities of WT and qv^{3J} mouse heart total lysate (n=4 mouse hearts/genotype) were analyzed by immunoblot. Band densities from non-saturated immunoblots of **(A)** Ankyrin-G, **(B)** $Na_v1.5$, **(C)** β_{IV} -spectrin, **(D)** n-cadherin, **(E)** β -catenin, and **(F)** CaMKII δ were measured with Adobe Photoshop 9.0, normalized to actin (loading control), and expressed as arbitrary units relative to expression in WT animals. CaMKII δ expression was decreased in qv^{3J} compared to WT (*p<0.05).

Figure S4. β_{IV} -spectrin immunostaining in heart tissue of WT and qv^{3J} mouse. β_{IV} -spectrin (*blue*) was localized to the intercalated disc (*white arrowheads*) of both WT and qv^{3J} heart sections.

Figure S5. qv^{3J} mice display selective loss of CaMKII δ immunostaining at the intercalated disc. WT (**A, D-E**) and qv^{3J} (**B-C, F-G**) mouse heart sections immunolabeled with antibodies against CaMKII δ (*red*) and resident intercalated disc protein connexin43 (*green*). Bottom panels (**D-G**) are magnified intercalated disc regions from different WT and qv^{3J} mice. Note that CaMKII δ is localized to both the intercalated disc (*white arrowheads*) and transverse-tubules (Z-line) of WT hearts. In contrast, while CaMKII δ transverse-tubule staining is retained in qv^{3J} hearts, CaMKII δ staining at the qv^{3J} intercalated disc was absent or just above background (decreased $89.2 \pm 5.3\%$ in qv^{3J} sections, $n=11$ measurements/genotype, $p < 0.05$).

Figure S6. Total myocyte potassium current and I_{to} are unchanged in WT and qv^{3J} cardiomyocytes. (**A**) Total myocyte potassium current density and (**B**) current density of the primary murine repolarizing current, the transient outward K^+ current (I_{to}) were measured in WT (*black*) and qv^{3J} (*red*) ventricular cardiomyocytes. There was no difference either total K^+ current or I_{to} at any voltage from -40 mV to 80 mV ($n=12$ /genotype, $p = N.S.$).

Figure S7. S571 in Na_v1.5 DI-DII loop is a CaMKII phosphorylation site. CaMKII phosphorylation assay on DI-DII intracellular domain of Nav1.5 (DI-DII) and DI-DII loop

engineered to harbor serine-to-alanine point mutation at S571 (DI-DII S571A). Cav1.2 β 2a subunit was used as positive control.

Figure S8. qv^{3J} heart lysates display reduced phospho- $Na_v1.5$ (S571) levels by immunoblot. Densitometric measurements in WT and qv^{3J} mouse hearts show a significant reduction in phospho- $Na_v1.5$ (S571) levels in qv^{3J} compared to WT mouse hearts (n=4 mice/genotype, $p < 0.01$). Data (arbitrary units) are corrected for protein levels by normalizing to actin. Note that total $Na_v1.5$ levels are unchanged between WT and qv^{3J} mouse hearts ($p = \text{NS}$, Fig.5).

Figure S9. Persistent I_{Na} in murine cardiomyocytes is rate dependent. Persistent I_{Na} in WT mouse cardiomyocytes measured at pacing frequencies of 0.5, 1, 2, and 4 Hz (* $p < 0.05$ vs. 0.5 hertz; # $p < 0.05$ vs. 1 Hz; $\Delta p < 0.05$ vs. 2 Hz).

Figure S10. Action potential duration at 90%, 75%, and 50% repolarization (APD_{90} , APD_{75} , APD_{50}) in WT and qv^{3J} cardiomyocytes at baseline and in the presence of 1 μM isoproterenol (pacing frequency = 0.5 Hz, n=14 WT, 16 qv^{3J} , * $p < 0.05$).

Figure S11. Equal I_{Na} density in large and small capacitance ventricular cardiomyocytes. Control experiments were performed on small and large capacitance cells to ensure adequate space clamp conditions (n=5 myocytes/group; $p < 0.05$). We observed equal I_{Na} density in smaller and larger capacitance cells confirming our ability to measure total available I_{Na} in our experiments.